

DOI: 10.1002/cplu.201300105

Mesostructured Dihydroxy-Functionalized Guanidinium-Based Polyoxometalate with Enhanced Heterogeneous Catalytic Activity in Epoxidation

Guojian Chen, Yu Zhou, Pingping Zhao, Zhouyang Long, and Jun Wang^{*[a]}

A mesostructured ionic liquid–polyoxometalate (IL-POM) hybrid has been prepared through designing a new dihydroxy-tethered guanidinium-based IL, *N'*-(2,3-dihydroxypropyl)-*N,N,N',N'*-tetramethylguanidinium chloride, to interact with Keggin-type POM phosphotungstic acid (H₃PW) in a self-assembly process. Scanning electron microscopy and transmission electron microscopy showed its special coral-shaped micro-morphology. Nitrogen sorption analysis indicated the formation of a porous structure with a moderate surface area of about 30 m²g⁻¹ and narrowly distributed pore size located in

the mesoscale. Assessed in the *cis*-cyclooctene epoxidation with H₂O₂, the mesostructured hybrid exhibited superior heterogeneous catalytic activity and steady reusability, and the conversion was more than four times that of homogeneous H₃PW itself, and more than 14 times that of the nonporous analogues. On the basis of the experimental results, a unique “substrate–solvent–catalyst” synergistic mechanism is proposed and discussed for understanding the dramatically enhanced catalytic performance.

Introduction

Polyoxometalates (POMs), a family of structurally diverse transition-metal oxygen anion clusters, have achieved wide applications in catalysis, materials science, biology, and magnetism.^[1] Intrinsically possessing controllable redox properties, various POMs have been used extensively as efficient homogeneous catalysts in many oxidative reactions, including the epoxidation of olefins to epoxides, which are important intermediates in fine-chemical and polymer synthesis.^[2] Nonetheless, pure POMs are soluble in many polar solvents, which causes difficulty in separation and recycling of the catalysts; therefore, many efforts have been made to prepare heterogeneous POM-based catalysts, such as immobilization of POMs on various porous supports, for example, silica-based matrices and organic polymers,^[3] and assembly of POMs with appropriate organic counter cations.^[4] The former favors higher surface areas to accelerate the mass transfer, and the latter is beneficial for adjusting the solubility, redox properties, and surface microenvironment of POM catalysts through modifying POMs with diverse organic cations. However, the self-assembled POM hybrids are frequently nonporous,^[5] thus limiting the heterogeneous catalytic activity in mass-transfer-controlled systems. Therefore, it is necessary to develop new methods to generate suitable micro/mesostructures on these POM materials.

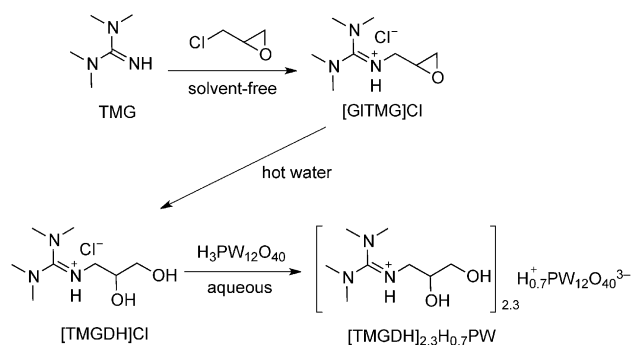
Ionic liquids (ILs) have received increasing attention as reaction media/catalysts in organic syntheses,^[6] as well as templates or building blocks for constructing inorganic–organic hybrid materials.^[7] Further, ILs have been used as adjustable counter cations of POM cluster anions to obtain a family of IL-POM hybrids applied in electrochemistry, catalysis, materials science, and so forth.^[8] In the field of catalysis, several IL-POMs have been reported as efficient homogeneous or phase-separation catalysts for epoxidation.^[9,10] In addition, our group has developed a “task-specific” IL-POM series through elaborate functionalized IL cations,^[11] and most of them exhibit superior catalytic performance in H₂O₂-based liquid-phase organic oxidation reactions. Nonetheless, little research has been directed towards the morphology and pore structure control of these hybrid catalysts. The difficulty is how to design suitable ILs that can self-assemble with the POM anion to create and control the porosity and accompanying morphology.

Among numerous ILs, guanidinium-based ILs (GILs) are of great interest for self-assembly synthesis, because the flexible tunability of guanidinium provides great opportunities for preparing a diverse range of cationic structures, and the planar C=N π-conjugated structure exhibits excellent thermal and robust chemical stabilities.^[12] However, previous reports have only introduced polyethylene glycol/ether, –SO₃H, and olefinic units as the functional groups to modify guanidinium cations,^[13] thus leaving room to develop new task-specific GILs for creating IL-POM hybrid catalysts.

Herein, a new dihydroxy-functionalized guanidinium IL, *N'*-(2,3-dihydroxypropyl)-*N,N,N',N'*-tetramethylguanidinium chloride ([TMGDH]Cl), is designed to fabricate a mesoporous IL-POM hybrid through ion exchange with the commercial Keggin-type POM H₃PW₁₂O₄₀ (H₃PW = phosphotungstic acid;

[a] G. Chen, Dr. Y. Zhou, P. Zhao, Z. Long, Prof. Dr. J. Wang
State Key Laboratory of Materials-Oriented Chemical Engineering
College of Chemistry and Chemical Engineering
Nanjing University of Technology
Nanjing, Jiangsu 210009 (P. R. China)
Fax: (+86) 25-83172264
E-mail: junwang@njut.edu.cn

 Supporting information for this article is available on the WWW under <http://dx.doi.org/10.1002/cplu.201300105>.



Scheme 1. Synthesis of dihydroxy-tethered guanidinium-based polyoxometalate $[\text{TMGDH}]_{2.3}\text{H}_{0.7}\text{PW}$. $[\text{GITMG}]\text{Cl} = N''\text{-glycidyl-}N,N,N',N'\text{-tetramethylguanidinium chloride}$.

Scheme 1). The dihydroxy group is introduced for two purposes. One is to control the morphology and pore structure of the obtained IL-POM hybrid. The other is to improve the catalytic performance, because it has been reported for epoxidation of olefins with H_2O_2 that introducing hydroxyl groups onto the surface of heterogeneous catalysts can enhance the catalytic activity,^[14] and the hydrogen bonding involved in the active metal-peroxo species in the presence of protic solvents has been regarded as a crucial catalytic promoter.^[15] The catalyst is characterized by ^1H NMR, ^{13}C NMR, FTIR, UV/Vis, and ESR spectroscopy, SEM, TEM, XRD, thermogravimetry (TG), nitrogen sorption, and elemental analysis, and its heterogeneous catalytic performance is assessed in the liquid-phase epoxidation of *cis*-cyclooctene with H_2O_2 . Various control catalysts are also prepared and tested for comparison. A unique “substrate–solvent–catalyst” mechanism is proposed to understand the superior catalytic performance of the material.

Results and Discussion

Formation of mesostructured GIL-POM catalysts

The mesoporous dihydroxy-tethered GIL-POM catalyst, denoted as $[\text{TMGDH}]_{2.3}\text{H}_{0.7}\text{PW}$, is prepared through the reaction between $[\text{TMGDH}]\text{Cl}$ and H_3PW in aqueous solution.

SEM images (Figure 1 A,B) indicate that the primary particles of $[\text{TMGDH}]_{2.3}\text{H}_{0.7}\text{PW}$ have a flexible noodle shape with a diameter of about 20 nm and a length of tens of nanometers, and these noodles are intertwined with each other to form a netlike substructure (Figure 1 A) with a nanoscale hollow structure and irregular coral-shaped morphology at the micrometer level. Figure 1 C and D show high-resolution TEM (HRTEM) images of $[\text{TMGDH}]_{2.3}\text{H}_{0.7}\text{PW}$, which confirm the existence of random mesopores in coral-shaped particles and micropores in the primary particles. However, the size of these micropores is too small

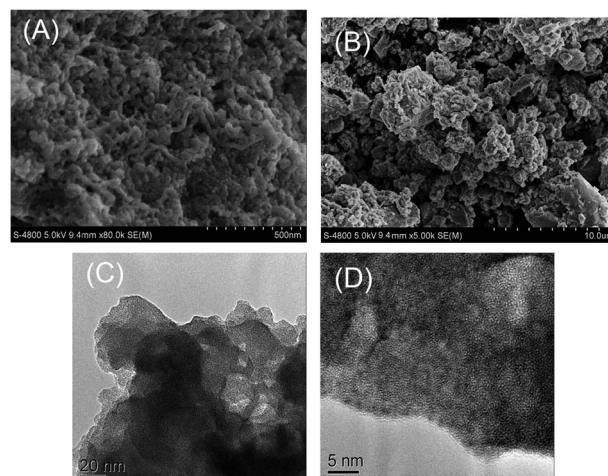


Figure 1. A,B) SEM and C,D) HRTEM images of $[\text{TMGDH}]_{2.3}\text{H}_{0.7}\text{PW}$.

(0.4 nm) to contribute any additional surface area when tested by nitrogen physisorption.

During the synthesis of the catalysts, it was found that the dihydroxy-tethered group in the IL cation plays a key role in the formation of the above special morphology. For example, similar primary particles and micromorphology along with clear channels and cavities are observed in $[\text{TMGDH}]_3\text{PW}$ (Figure 2 A), which is also prepared by employing the same IL

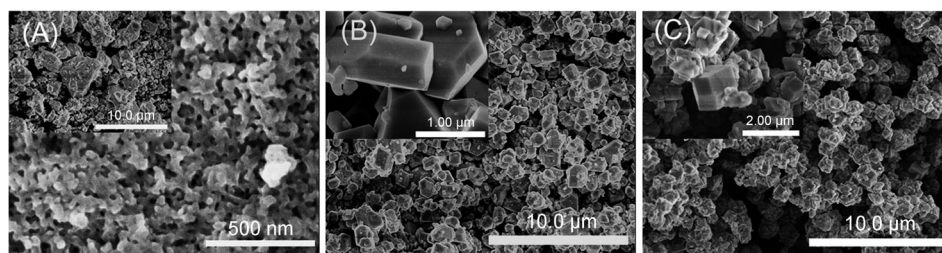


Figure 2. SEM images of A) $[\text{TMGDH}]_3\text{PW}$, B) $[\text{TMGOH}]_{2.2}\text{H}_{0.8}\text{PW}$, and C) $[\text{TMG}]_3\text{PW}$.

$[\text{TMGDH}]\text{Cl}$ but with Na_3PW ; nonetheless, the packing of primary particles is closer than for $[\text{TMGDH}]_{2.3}\text{H}_{0.7}\text{PW}$. On the contrary, the morphology changes to smooth angular blocks with a size in micrometers by using monohydroxy-tethered and hydroxy-free GIL cations to prepare $[\text{TMGOH}]_{2.2}\text{H}_{0.8}\text{PW}$ and $[\text{TMG}]_3\text{PW}$ hybrids (Figure 2 B,C), and no substructure can be identified.

The surface area and pore structure are further characterized by nitrogen sorption experiments. As shown in Figure 3 A, curve a, the nitrogen sorption isotherm of $[\text{TMGDH}]_{2.3}\text{H}_{0.7}\text{PW}$ is type IV with a clear H1-type hysteresis loop in the partial pressure range of $P/P_0 = 0.5\text{--}0.9$, characteristic of a mesoporous material. Curve a in Figure 3 B gives the pore size distribution of $[\text{TMGDH}]_{2.3}\text{H}_{0.7}\text{PW}$ calculated by the Barrett–Joyner–Halenda method, which shows a narrow pore size distribution with the most probable pore size of 6.2 nm, in agreement with the result of the TEM image. Table 1 lists the surface areas, pore

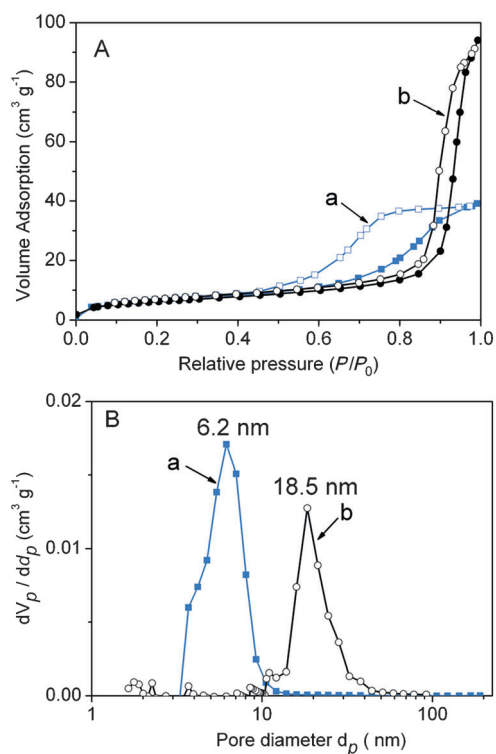


Figure 3. A) N₂ sorption isotherms and B) pore size distribution of a) [TMGDH]_{2.3}H_{0.7}PW and b) [TMGDH]₃PW.

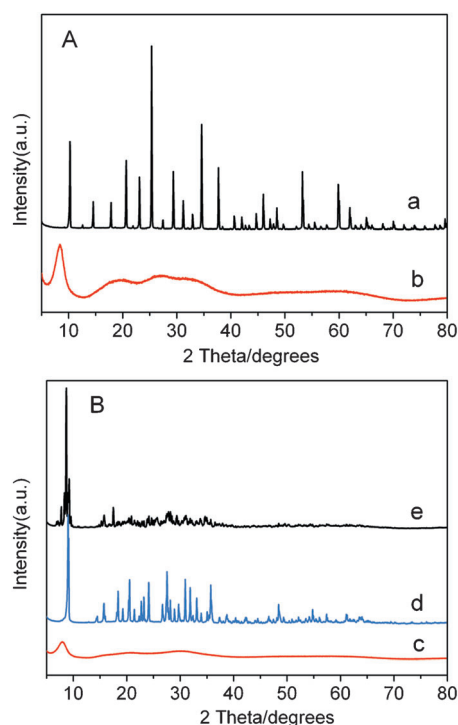


Figure 4. XRD patterns of A) a) H₃PW₁₂O₄₀, b) [TMGDH]_{2.3}H_{0.7}PW; B) c) [TMGDH]₃PW, d) [TMGOH]_{2.2}H_{0.8}PW, and e) [TMG]₃PW.

Table 1. Textural properties and catalytic performances of POM catalysts in the epoxidation of *cis*-cyclooctene with H₂O₂.^[d]

Entry	Catalyst	S _{BET} ^[a] [m ² g ⁻¹]	V _p ^[b] [cm ³ g ⁻¹]	D _{av} ^[c] [nm]	Solubility in reaction	Conversion ^[e] [%]	Selectivity ^[f] [%]
1	[TMGDH]Cl	–	–	–	soluble	0	–
2	H ₃ PW	5.4	–	–	soluble	22.3	84.7
3	[TMGDH] _{2.3} H _{0.7} PW	28.0	0.06	10.4	insoluble	99.5	98.5
4	[TMGDH] ₃ PW	22.6	0.14	25.5	insoluble	96.5	99.0
5	[TMGOH] _{2.2} H _{0.8} PW	2.1	–	–	insoluble	6.5	100
6	[TMG] ₃ PW	0.3	–	–	insoluble	7.0	100
7	30% H ₃ PW/SiO ₂ ^[g]	204	0.56	7.0	insoluble	74.4	31.6

[a] BET surface area. [b] Total pore volume. [c] Average pore size. [d] Reaction conditions: *cis*-cyclooctene (10 mmol), 30 wt% H₂O₂ (5 mmol), catalyst (0.1 g), solvent (methanol, 3 mL), 60 °C, 6 h. [e] Conversion based on H₂O₂. [f] Selectivity for 1,2-epoxycyclooctane; by-products: 2-cycloocten-1-ol, 2-cycloocten-1-one, and 1,2-cyclooctanediol. [g] The amount of 30% H₃PW/SiO₂ was 0.3 g.

volumes, and average pore sizes. The results indicate that [TMGDH]_{2.3}H_{0.7}PW has a moderate BET surface area of 28 m² g⁻¹, close to that of the previously reported polyammonium-POM hybrid mesoporous materials or a peroxophosphotungstate-based polymer-immobilized IL-phase catalyst with surface area of 27–51 m² g⁻¹.^[3c,4a] Also, the sample [TMGDH]₃PW prepared from the same IL as [TMGDH]_{2.3}H_{0.7}PW shows a type IV nitrogen sorption isotherm with H1-type hysteresis loop in a relatively higher partial pressure range of P/P₀=0.8–0.99, which corresponds to a surface area of 22.6 m² g⁻¹ (Table 1) and a larger pore size most probably of

18.5 nm (Figure 3 B, curve b). However, the other samples prepared from monohydroxy-tethered and hydroxy-free GIL cations all exhibit very small surface area, even lower than that of H₃PW itself (Table 1).

Figure 4 shows the XRD patterns of various GIL-POM hybrids. The XRD pattern of H₃PW₁₂O₄₀ presents a number of sharp Bragg peaks, characteristic of Keggin-type phosphotungstate (PW),^[16] but these peaks disappear after combining with IL cation [TMGDH]⁺ (Figure 4A). For [TMGDH]_{2.3}H_{0.7}PW and [TMGDH]₃PW samples, a new broad Bragg reflection is visible

at 2θ=8.2°, with a d spacing of 1.08 nm, close to the size of a basic structural unit of IL-POM.^[17] This phenomenon is in accordance with the result of the HRTEM image (Figure 1 D), in which the primary structural units (ca. 1.1 nm) are distributed homogeneously throughout the IL-POM secondary structures to form uniform wormlike small micropores, which correspond to the residual voids of ion-pair assembly.^[18] In addition, many new characteristic peaks appear in the XRD patterns of [TMGOH]_{2.2}H_{0.8}PW and [TMG]₃PW (Figure 4B), thus indicating the formation of new three-dimensional crystal structures assembled by Keggin anions with GIL cations,^[11d,19] in good

agreement with the polyhedral morphologies of their SEM images.

Further characterization of [TMGDH]_{2.3}H_{0.7}PW

The hybrid [TMGDH]_{2.3}H_{0.7}PW was further characterized by elemental analysis, TG, and ¹H NMR, ¹³C NMR, FTIR, UV/Vis, and ESR spectroscopy. The elemental analysis found (wt%) C 6.79, N 2.90, and H 1.56, close to the calculated values of C 6.67, N 2.92, and H 1.39, thus indicating the formula of [TMGDH]_{2.3}H_{0.7}PW shown in Scheme 1. The structure of the sample was further confirmed by ¹H and ¹³C NMR spectroscopy (see Figure S1 in the Supporting Information). Particularly, in the ¹H NMR spectra, the signals for [TMGDH]Cl at δ = 6.66 (OH) and 8.11 ppm (NH) shift to δ = 6.23 (OH) and 7.78 ppm (NH) for [TMGDH]_{2.3}H_{0.7}PW, respectively, thus implying the existence of active protons in the latter sample. The above phenomenon strongly demonstrates that the counter protons of the POM anion have not been totally exchanged by GIL cations in the ion-exchange process, probably because of the strong acidic environment relative to H₃PW₁₂O₄₀.^[11c] The TG curve (see Figure S2 in the Supporting Information) indicates a thermally stable structure for [TMGDH]_{2.3}H_{0.7}PW up to 240 °C. The slight weight loss at the early heating stage below 200 °C results from the release of moisture and constitutional water, whereas the drastic weight loss in the range 240–600 °C is assigned to the decomposition of the hydroxy-attached TMG moiety plus the complete collapse of the inorganic Keggin PW structure with the formation of P₂O₅ and WO₃.^[20] Moreover, the total weight loss of about 13.30% in the range 240–600 °C is very close to the value of 13.20% calculated theoretically from elemental analysis, once again verifying the chemical composition of [TMGDH]_{2.3}H_{0.7}PW.

Figure 5 shows the FTIR spectra of H₃PW₁₂O₄₀ and [TMGDH]_{2.3}H_{0.7}PW. The spectrum of H₃PW₁₂O₄₀ possesses vibration bands characteristic of the Keggin anion located at 1080, 983, 889, and 803 cm⁻¹, corresponding to vibrations ν (P–O_a), ν (W=O_t), ν (W–O_b–W), and ν (W–O_c–W), respectively.^[21] Nonetheless, these four characteristic peaks for the Keggin structure occur with light shifts on [TMGDH]_{2.3}H_{0.7}PW, which indicates strong ionic interactions between the [TMGDH]⁺ and PW₁₂O₄₀³⁻ and thus the formation of the IL-POM hybrid. In ad-

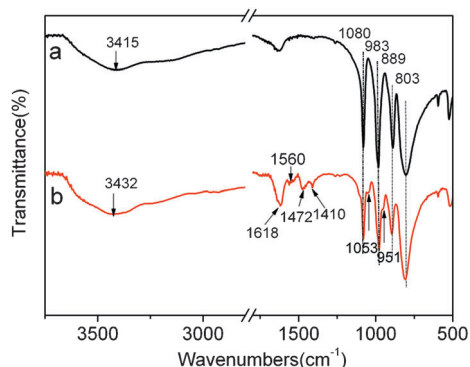


Figure 5. FTIR spectra of a) H₃PW₁₂O₄₀ and b) [TMGDH]_{2.3}H_{0.7}PW.

dition, several new peaks emerge on the spectrum of [TMGDH]_{2.3}H_{0.7}PW. The weak band at 1053 cm⁻¹ is a branched peak from the stretching P–O vibration band at 1079 cm⁻¹, which implies the distortion of the symmetric Keggin framework owing to the partial degradation of the pH-sensitive PW₁₂O₄₀³⁻ anion in IL aqueous solution.^[22] Another weaker band at 951 cm⁻¹ is assigned to the split peak from the vibration of W^{VI}=O at 979 cm⁻¹, which suggests the existence of reduced W⁵⁺ species as a result of the intramolecular charge transfer from the π -conjugated TMG moiety to terminal W^{VI}=O.^[23] Other new peaks at 2964, 1618, 1560, 1472, and 1410 cm⁻¹ are assigned to the TMG moiety.^[24] The strong and broad peak at 3432 cm⁻¹ is assigned to the stretching vibration of O–H in [TMGDH]⁺, thereby indicating the existence of multiple hydrogen-bonding networks in the IL-POM hybrid.^[25] The hydrogen-bonding interactions may account for the solid nature of [TMGDH]_{2.3}H_{0.7}PW with a high melting point of approximately 250 °C. In addition, [TMGDH]_{2.3}H_{0.7}PW is insoluble in most common solvents, including water, alcohols, ethyl acetate, acetic acid, acetone, acetonitrile, and DMF, and is only sparingly soluble in DMSO.

Figure 6 depicts the UV/Vis and ESR spectra of [TMGDH]_{2.3}H_{0.7}PW and pure H₃PW₁₂O₄₀, which is applied to reflect the electronic behavior of catalysts. In the UV/Vis spectrum of [TMGDH]_{2.3}H_{0.7}PW, a broad absorption band in the range of 600–800 nm is assignable to the intramolecular charge transfer from W⁶⁺ to W⁵⁺ (Figure 6A, curve a),^[26] but the band was undetectable for H₃PW₁₂O₄₀ (Figure 6A, curve b). The ESR signals at 3500 G on curve a in Figure 6B also reveal the existence of the low-valent W⁵⁺ species in the hybrid

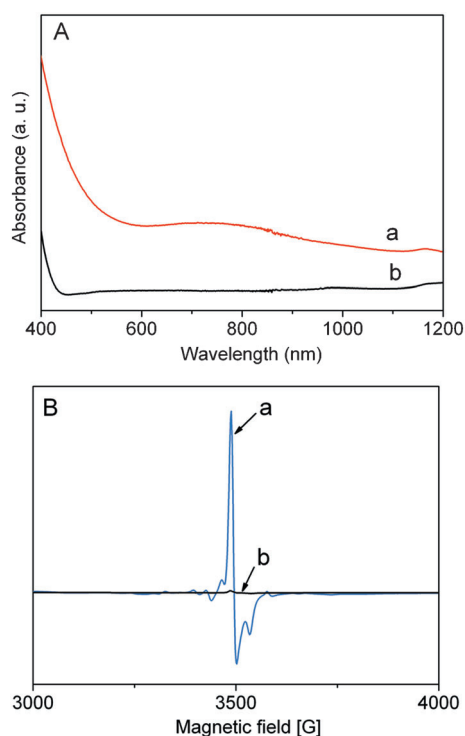


Figure 6. A) UV/Vis and B) ESR spectra of a) [TMGDH]_{2.3}H_{0.7}PW and b) H₃PW₁₂O₄₀.

[TMGDH]_{2,3}H_{0,7}PW, and curve b indicates the absence of W⁵⁺ species in pure H₃PW₁₂O₄₀. These phenomena plus the results from IR spectra sufficiently confirm the formation of W⁵⁺ species during the ion exchange of [TMGDH]Cl and H₃PW₁₂O₄₀.

Catalytic activity in the epoxidation reaction

The catalytic performances of various catalysts are assessed in the epoxidation of the probe substrate *cis*-cyclooctene with aqueous H₂O₂ as oxidant and methanol as solvent. As shown in Table 1, the neat precursors IL [TMGDH]Cl and POM H₃PW dissolve in the reaction medium to give a homogeneous system, but their catalytic activities are very low (Table 1, entries 1 and 2): no product is detected by using [TMGDH]Cl, and low conversion of 22.3% and selectivity of 84.7% are observed by using H₃PW. In contrast, the hybrid catalyst [TMGDH]_{2,3}H_{0,7}PW is insoluble and well dispersed in the oxidative reaction medium, thus leading to a heterogeneous system and exhibiting a high conversion of 99.5% and selectivity of 98.5% (Table 1, entry 3) under the optimized reaction conditions. The heterogeneous catalyst [TMGDH]_{2,3}H_{0,7}PW can be recovered simply by filtration after reaction, and the catalytic reusability was measured by a five-run test without adding any fresh catalyst after each run. As shown in Figure S3, there was no significant loss of conversion and selectivity after five runs, which implied good reusability of this catalyst.

On the contrary, nonporous catalysts [TMGOH]_{2,2}H_{0,8}PW and [TMG]₃PW with very small surface areas all give poor conversions of 6.5 and 7.0%, respectively (Table 1, entries 5 and 6), even lower than that of homogeneous H₃PW. The above phenomenon suggests that the morphology and porous structure play an important role in this reaction. To support this deduction, the proton-free counterpart [TMGDH]₃PW with similar morphology and mesostructure to [TMGDH]_{2,3}H_{0,7}PW was tested, which also offered comparably a high conversion of 96.5% and selectivity of 99.0%. These results indicate that the coral-shaped morphology and accompanying mesostructure favor a better catalytic performance. Moreover, this control experiment also reveals that the protonation of [TMGDH]_{2,3}H_{0,7}PW is not the key contribution to the superior catalytic performance, little different from that in the previous report.^[11c] Notably, the self-formed mesostructure in [TMGDH]_{2,3}H_{0,7}PW or [TMGDH]₃PW possesses unique advantages for the epoxidation reaction. For example, 30% H₃PW/SiO₂ obtained through directly impregnating H₃PW on the hydroxy-enriched porous silica support only gives a moderate conversion of 74.4% but with a low selectivity of 31.6% (Table 1, entry 7), owing to the hydration of epoxide to diol in the protonated hydroxy acidic conditions and allylic oxidation in the homolytic pathway.^[27]

Solvent effects in the epoxidation reaction

As shown in Figure 7A, the catalyst [TMGDH]_{2,3}H_{0,7}PW exhibits different performances in the epoxidation of *cis*-cyclooctene with H₂O₂ by using various solvents. During the reaction, the catalyst is insoluble in all the solvents. Acetonitrile and ethyl acetate are the two commonly used good solvents in many

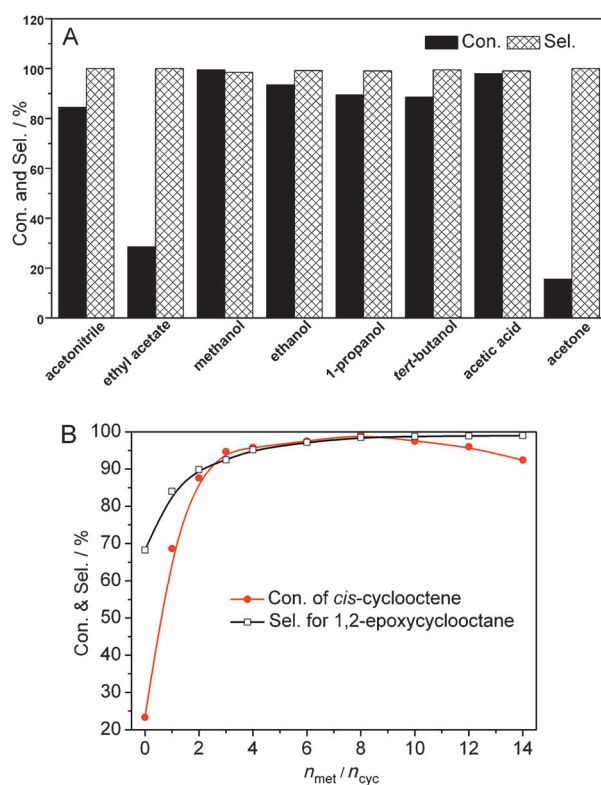


Figure 7. A) Catalytic performance in epoxidation of *cis*-cyclooctene with H₂O₂ in different solvents. B) Influence of different molar ratios of methanol to *cis*-cyclooctene ($n_{\text{met}}/n_{\text{cyc}}$). Reaction conditions: *cis*-cyclooctene (10 mmol), 30 wt% H₂O₂ (5 mmol), catalyst [TMGDH]_{2,3}H_{0,7}PW (0.1 g), solvent (3 mL), 60 °C, 6 h. Con. = conversion, Sel. = selectivity.

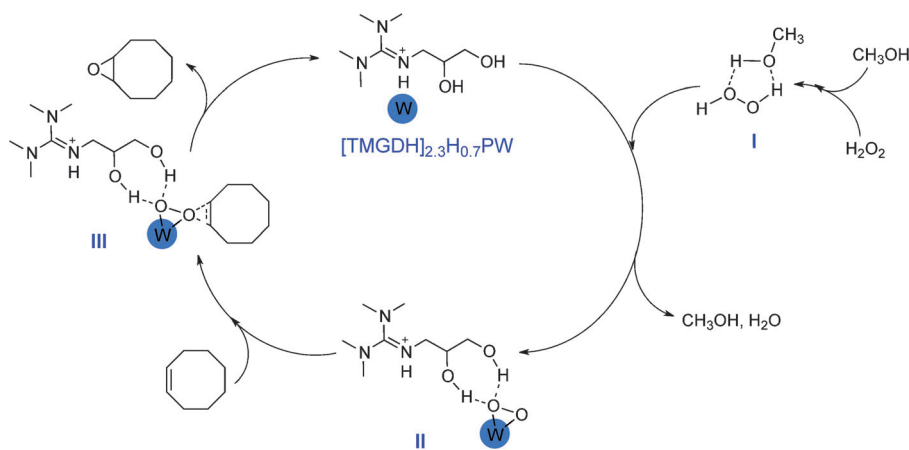
POM-catalyzed epoxidation reactions of olefins.^[28] Nonetheless, modest conversion of 84.6% and low conversion of 28.5% are obtained by acetonitrile and ethyl acetate, respectively. Interestingly, high conversions are obtained by using short-chain aliphatic alcohol solvents. Among them, methanol provides the highest conversion of 99.5% and selectivity of 98.5%. On increasing the carbon chain length of aliphatic alcohols, the conversions continuously decrease to 93.4% for ethanol, 89.5% for 1-propanol, and 88.6% for *tert*-butyl alcohol. Note that these short-chain alcohols are hardly oxidized by using PW anions as catalysts in mild conditions,^[29] thus avoiding the possible role of “sacrificial” solvents in our reaction.^[30] In addition, a common polar protic solvent, acetic acid, was employed, which achieved a good conversion of 98.0% and selectivity of 99.0%, whereas a typical aprotic solvent, acetone, only gives a very low conversion of 15.6%. According to the above results and referring to Kamlet–Taft plots,^[31] it is found that “greener” protic solvents with moderate polarity facilitate good performance in our reaction system.

The influence of the solvent amount was also tested with methanol. As shown in Figure 7B, the conversion is only 23.4% with low selectivity of 68.2% in the solvent-free reaction. When methanol is used as solvent, both conversion and selectivity gradually increase along with the enhancement of the molar ratio of methanol to *cis*-cyclooctene ($n_{\text{met}}/n_{\text{cyc}}$), thereby achieving the highest value as $n_{\text{met}}/n_{\text{cyc}}$ stays on 8. Under these

conditions, the reaction is a liquid–liquid–solid triphasic system, because such a low amount of methanol is unable to completely homogenize the organic phase of *cis*-cyclooctene. On further increasing the methanol amount, the reaction system tends to a liquid–solid biphasic state owing to the gradual solution of *cis*-cyclooctene in methanol; however, the conversion decreases though the selectivity is unchanged. When the value of $n_{\text{met}}/n_{\text{cyc}}$ is 14, the amount of methanol is enough to dissolve all the *cis*-cyclooctene to give a liquid–solid heterogeneous system; but the conversion is only 92.4%. In previous works, a large volume of solvent was usually used for homogenizing substrates,^[10a,32] yet, in our experiment, a special phenomenon is observed that a relatively small solvent/substrate molar ratio favors higher conversion.

Substrate–solvent–catalyst mechanism

Based on the above results and previous studies on epoxidation of olefins, a “substrate–solvent–catalyst” reaction mechanism is proposed in Scheme 2 to understand the superior per-



Scheme 2. Proposed catalytic mechanism for [TMGDH]_{2.3}H_{0.7}PW-catalyzed epoxidation of *cis*-cyclooctene with H₂O₂ in solvent CH₃OH.

formance of the catalyst [TMGDH]_{2.3}H_{0.7}PW. Previous works on PW-based catalysts indicate that tungsten-peroxo complex is the catalytically active site for epoxidation of olefins, and the epoxidation process usually proceeded in three steps: 1) the formation of tungsten-peroxo complex through the interaction between PW species and H₂O₂; 2) attack of the olefin substrate by the tungsten-peroxo complex, to generate the epoxide product; and 3) regeneration of the PW species.^[33] Besides, the solvent will take part in the formation of the peroxo complex through involving the interaction between the substrate and H₂O₂.^[34] As shown in Scheme 2, the epoxidation of *cis*-cyclooctene catalyzed by [TMGDH]_{2.3}H_{0.7}PW also undergoes three steps. First, the five-membered ring structure I is formed through the hydrogen-bonding interaction between H₂O₂ and the hydroxyl group of methanol.^[35] Then the H₂O₂ molecules incorporated in complex I contact the Keggin-framework

W sites to create the {PO₄[WO(O₂)₂]₄}³⁻-containing tungsten-peroxo complex II.^[33b] Afterwards, the substrate *cis*-cyclooctene attacks the tungsten-peroxo species in II to generate the possible tungsten-peroxo-cyclooctene intermediate structure III, then gives the corresponding epoxide product along with the final regeneration of the original catalyst. Different from a homogeneous reaction, mass transfer is an important factor in the heterocatalytic process, involving the influences of morphology and pore structure, and the substrate–solvent–catalyst interaction.

As described in Scheme 2, several steps are related to the mass-transfer process, for example, the attack of complex I to W sites and the accessing process of *cis*-cyclooctene to the tungsten-peroxo species in II. In these processes, the behavior of the catalytically active sites is limited by the mass-transfer efficiency, and thus the morphology and mesostructure play a key role in the reaction. Generally, loosely packed nanoparticles with moderate mesopores favor fast mass transfer and the exposure of catalytically active sites on internal surfaces. Therefore, the mesostructured samples ([TMGDH]_{2.3}H_{0.7}PW and [TMGDH]₃PW) with coral-shaped morphology all exhibit superior catalytic performances (Table 1).

In detail, *cis*-cyclooctene and H₂O₂ molecules in methanol solvent diffuse easily into the internal surface of the solid catalyst through the mesopores, and the nanocavities among POM anions allow good access of substrates and H₂O₂ to W species in the POM anion, which accelerates mass transfer and the formation of the catalytically active species tungsten-peroxo complex II. On the contrary, the catalytic epoxidation activities of nonporous samples ([TMGOH]_{2.2}H_{0.8}PW and [TMG]₃PW) with bulky block-shaped morphology are always very low (Table 1), in spite of

having crystal structures. Therefore, fabricating suitable micro/mesostructures for IL-POM catalysts is crucial for superior catalytic activity.

The substrate–solvent–catalyst interaction is another important factor that influences the mass transfer. In a hetero system, the substrates and catalyst are all surrounded by the solvent, and a suitable solvent benefits the access of the substrate to the catalyst and the reduction of the activation barrier through the substrate–solvent–catalyst interaction. Thus, the conversion varies with different solvents. When protic polar solvents such as methanol are used, strong hydrogen-bonding interactions will form between solvent molecules and H₂O₂, as well as the introduced hydroxyl groups in the catalyst, which would thus decrease the adsorption resistance and benefit the access of the substrate to the active site in the catalyst. Besides, many previous reports indicate that the hydrogen-bond-

ing networks in the "CH₃OH–H₂O₂" complex can accelerate the activation of H₂O₂ in metal-based oxidations through reducing the catalytic activation barrier.^[35,36] Therefore, H₂O₂ has been preliminarily activated by the formation of hydrogen bonds in structure I before attacking the W sites, and thus the solvent–oxidant interaction may be responsible for the extremely high catalytic performance in the epoxidation of *cis*-cyclooctene with H₂O₂ when methanol (or other protic polar solvent such as acetic acid) is used as solvent (Figure 7A). Furthermore, recent reports^[14] have revealed the promotional functionality of the hydroxyl groups or functionalized protic molecules introduced on the surface of heterogeneous catalysts, such as Ti-COE-4 and Ti-SBA-15, for epoxidations with H₂O₂. For the above reasons, the abundant hydroxyl groups in [TMGDH]_{2,3}H_{0,7}PW are not only able to promote the accessibility through the solvent–catalyst interaction, but are also beneficial for the formation and stability of tungsten-peroxo species in catalytically active complex II.

Moreover, the solvent amount determines the concentration of substrate, and the mass transfer of substrate seems not to be hindered by a smaller amount of solvent and highly concentrated substrate. As shown in Figure 7B, a suitable amount of methanol solvent (8.0 molar equiv with respect to *cis*-cyclooctene) is required to obtain the high activity of 99.5% in a triphasic system. However, the catalytic activity is low in the absence of methanol, which is ascribed to the access difficulty of *cis*-cyclooctene to the catalyst. A very small amount of methanol ($n_{\text{met}}/n_{\text{cyc}}=2$) readily leads to a dramatically increased conversion of 87.6% owing to the enhancement of mass transfer. Excess methanol will reduce the concentration of substrate, and thus slow down the reactivity of *cis*-cyclooctene. The above phenomenon can be explained by mass-transfer efficiency and concentration effects by tuning a moderate amount of methanol.

Finally, it should be pointed out that intramolecular electron transfer from the GIL organic moiety to terminal W^{VI}=O in POM clusters is a prerequisite for high catalytic performance. This special electronic behavior leads to the coexistence of terminal W⁶⁺/W⁵⁺ species^[23,37] in [TMGDH]_{2,3}H_{0,7}PW, which should largely favor the redox property of W species for catalyzing the epoxidation reaction with H₂O₂ based on the active tungsten-peroxo complex II. Accordingly, the lack of favorable electron transfer from organic cations to POM units can be an interpretation for the low catalytic activity of *cis*-cyclooctene epoxidation with H₂O₂ over H₃PW/SiO₂ and H₃PW, though H₃PW/SiO₂ has a large surface area and the mass-transfer resistance is weaker if using a homogeneous H₃PW catalyst. However, for the nonporous IL-POM catalysts, such as [TMGOH]_{2,2}H_{0,8}PW and [TMG]₃PW, no matter whether they possess the reduced-state W⁵⁺ species (see ESR spectra in Figure S4), they all give low catalytic activities, because the morphology and porous structure of a catalyst affect significantly the accessibility of the H₂O₂ to W sites to form catalytically active W-peroxo species.

Briefly, it is the loosely packed nanoparticles with moderate mesopores that provide a suitable situation, in which the hydrogen-bonding-assisted substrate–solvent–catalyst synergistic catalytic mechanism can be applied to explain the high catalytic

activity of hydroxy-rich mesostructured [TMGDH]_{2,3}H_{0,7}PW hybrid in the epoxidation of *cis*-cyclooctene with H₂O₂ in protic solvents.

Conclusion

A novel mesostructured IL-POM hybrid has been self-assembled by ion exchange of a dihydroxy-containing guanidinium IL with phosphotungstic acid. The obtained hybrid material exhibits superior heterogeneous catalytic activity and steady reusability in the epoxidation of *cis*-cyclooctene with H₂O₂, as a result of the promotion of unusual morphology and pore structure, together with a hydrogen-bonding-enriched microenvironment surrounding the POM anion. Particularly, the controllable introduction of hydroxyl groups into IL cations not only favors the pore structure and morphology control of the IL-POM hybrid but also benefits the accessibility of active sites in POM-based catalysts.

Experimental Section

Materials and methods

All the chemicals were of analytical grade and used as received. FTIR spectra were recorded on a Nicolet 360 FTIR instrument (KBr disks) in the region 4000–400 cm⁻¹. Solid UV/Vis spectra were measured with a PE Lambda 950 spectrometer and BaSO₄ was used as an internal standard. ESR spectra were recorded on a Bruker EMX-10/12 spectrometer at the X-band. ¹H and ¹³C NMR spectra were measured with a Bruker DPX 500 spectrometer at ambient temperature in [D₆]DMSO by using TMS as internal reference. The CHN elemental analysis was performed on an elemental analyzer Vario EL cube. Melting points were determined using a ×4 digital microscopic melting point apparatus with an upper limit of 250 °C. TG analysis was performed with an STA409 instrument in dry air at a heating rate of 10 °C min⁻¹. XRD patterns were collected on a Bruker D8 Advance powder diffractometer using a Ni-filtered Cu_{Kα} radiation source at 40 kV and 20 mA, from 5 to 80° with a scan rate of 0.2° s⁻¹. SEM images were obtained on a Hitachi S-4800 field-emission scanning electron microscope. The TEM images were obtained by using a JEOL JEM-2010 (200 kV) TEM instrument. BET surface areas were measured at the temperature of liquid nitrogen (77 K) by using a Micromeritics ASAP2010 analyzer; the samples were degassed at 150 °C for 3 h to a vacuum of 10⁻³ Torr before analysis.

Catalyst preparation

The mesoporous dihydroxy-functionalized GIL-POM catalyst, denoted as [TMGDH]_{2,3}H_{0,7}PW, was prepared in three steps (Scheme 1).

First, *N'*-glycidyl-*N,N,N,N'*-tetramethylguanidinium chloride [GITMG]Cl was synthesized by direct N-alkylation of *N,N,N,N'*-tetramethylguanidine (TMG) with epichlorohydrin without solvent, based on the previously described method with slight modification.^[38] TMG (5.76 g, 50 mmol) and epichlorohydrin (5.55 g, 60 mmol) were added to a flask and stirred magnetically at 40 °C for 24 h under a nitrogen atmosphere. The white precipitate was isolated by filtration, washed with acetone (5 × 10 mL), and dried under vacuum to obtain a hygroscopic light yellow solid [GITMG]Cl with a yield of 70%.

Second, the dihydroxy-tethered IL N'' -(2,3-dihydroxypropyl)- N,N,N',N' -tetramethylguanidinium chloride [TMGDH]Cl was prepared by ring opening of [GITMG]Cl in hot water.^[39] [GITMG]Cl (1.0 g) was dissolved in water (20 mL), and the obtained mixture was heated at reflux with stirring at 70 °C for 24 h. After the reaction, water was removed by rotary evaporation and the product was dried under vacuum for 12 h. [TMGDH]Cl was obtained as a quite viscous light yellow oil at room temperature. [TMGDH]Cl: ¹H NMR (300 MHz, [D₆]DMSO, TMS): δ = 2.93 (s, 12H; N-CH₃), 3.41–3.75 (m, 5H; CH₂, CH), 5.01 (s broad, 1H; OH), 6.66 (s broad, 1H; OH), 8.11 ppm (s, 1H; NH); ¹³C NMR (75.5 MHz, [D₆]DMSO, TMS): δ = 39.50 (N-CH₃), 60.68 (CH₂), 65.89–67.19 (CH₂), 75.92 (CH), 160.90 ppm (C-N).

Finally, [TMGDH]_{2.3}H_{0.7}PW was prepared by reacting [TMGDH]Cl (3 mmol) with H₃PW₁₂O₄₀ (1 mmol) in aqueous solution stirred at room temperature for 24 h. The resulting light yellow precipitate was isolated by filtration, washed with water, and dried in a vacuum at 80 °C to give the final product with a yield of 94%. [TMGDH]_{2.3}H_{0.7}PW: ¹H NMR (300 MHz, [D₆]DMSO, TMS) (Figure S1 A): δ = 2.90 (s, 12H; N-CH₃), 3.50–3.80 (m, 5H; CH₂, CH), 4.93 (s broad, 1H; OH), 6.23 (s broad, 1H; OH), 7.78 ppm (s, 1H; NH); ¹³C NMR (75.5 MHz, [D₆]DMSO, TMS) (Figure S1 B): δ = 39.50 (N-CH₃), 52.09 (CH₂), 61.07 (CH₂), 67.80 (CH), 160.91 ppm (C=N); FTIR (KBr): $\tilde{\nu}$ = 3437, 2965, 1617, 1560, 1473, 1410, 1260, 1080, 979, 896, 808, 595, 520 cm⁻¹. In addition, the unprotonated [TMGDH]₃PW was prepared by similar procedures by anion exchange of [TMGDH]Cl with Na₃PW₁₂O₄₀ but with a low yield of 40%.

N'' -Ethanol- N,N,N',N' -tetramethylguanidinium bromide [TMGOH]Br was synthesized according to the previous literature.^[40] TMG (2.30 g, 20 mmol) and 2-bromoethanol (3.75 g, 30 mmol) were dissolved in ethanol (20 mL) and heated at reflux with stirring at 80 °C for 24 h. A colorless liquid was obtained by distilling the solvent and it was then solidified at room temperature. The white solid was washed thoroughly with diethyl ether (5 × 10 mL) and dried at 80 °C under vacuum for 24 h to obtain [TMGOH]Br with a modest yield of 80%.

The monohydroxy-tethered POM, a white solid assigned as [TMGOH]_{2.2}H_{0.8}PW, was synthesized similarly with a yield of 92%. FTIR (KBr): $\tilde{\nu}$ = 3465, 3368, 3257, 2938, 1639, 1618, 1561, 1459, 1411, 1078, 977, 895, 810, 595, 514 cm⁻¹; elemental analysis calcd (wt%): C 5.72, H 1.26, N 2.86; found: C 5.70, H 1.30, N 2.89. The hydroxy-free [TMG]₃PW was prepared by neutralization reaction of H₃PW₁₂O₄₀ (1 mmol) with TMG (3 mmol) in aqueous solution to give a white solid, yield 95%. FTIR (KBr): $\tilde{\nu}$ = 3455, 3367, 3252, 2940, 1617, 559, 1455, 1411, 1079, 978, 895, 810, 596, 520 cm⁻¹; elemental analysis calcd (wt%): C 5.62, H 1.30, N 3.91; found: C 5.68, H 1.30, N 3.95.

Catalytic tests

The catalytic performance was studied by a model reaction, the epoxidation of *cis*-cyclooctene with H₂O₂. In a typical run, *cis*-cyclooctene (10 mmol), methanol (3 mL), and catalyst [TMGDH]_{2.3}H_{0.7}PW (0.1 g, 0.03 mmol) were stirred in a flask at 60 °C for several minutes, and then 30 wt% aqueous H₂O₂ (5 mmol) was added drop by drop. The reaction was continued for 6 h with heating at reflux. Then the internal standard decane was added and the resulting mixture was diluted with methanol. The organic phase was collected and analyzed by gas chromatography, with an instrument (SP-6890A) equipped with a flame ionization detector and a capillary column (SE-54, 30 m × 0.32 mm × 0.3 μm). Conversion (based on H₂O₂) = (mmol *cis*-cyclooctene converted)/(mmol initial H₂O₂) ×

100%; selectivity of epoxide = (mmol epoxide)/(mmol *cis*-cyclooctene converted) × 100%. During reusability assessment, the catalyst was separated by filtration, washed with ethanol three times, dried in a vacuum at 80 °C for 6 h, and then used for the next run.

Acknowledgements

We are grateful to the Key Program of the National Natural Science Foundation of China (No. 21136005).

Keywords: epoxidation · heterogeneous catalysis · ionic liquids · morphology · polyoxometalates

- [1] D. Long, E. Burkholder, L. Cronin, *Chem. Soc. Rev.* **2007**, *36*, 105–121.
- [2] a) C. L. Hill, C. M. Prosser-McCarthy, *Coord. Chem. Rev.* **1995**, *143*, 407–455; b) N. Mizuno, K. Yamaguchi, K. Kamata, *Coord. Chem. Rev.* **2005**, *249*, 1944–1956.
- [3] a) K. Yamaguchi, C. Yoshida, S. Uchida, N. Mizuno, *J. Am. Chem. Soc.* **2005**, *127*, 530–531; b) S. P. Maradur, C. Jo, D. H. Choi, K. Kim, R. Ryoo, *ChemCatChem* **2011**, *3*, 1435–1438; c) S. Doherty, J. G. Knight, J. R. Ellison, D. Weekes, R. W. Harrington, C. Hardacre, H. Manyar, *Green Chem.* **2012**, *14*, 925–929; d) M. Carraro, G. Fiorani, L. Mognon, F. Caneva, M. Gardan, C. Maccato, M. Bonchio, *Chem. Eur. J.* **2012**, *18*, 13195–13202.
- [4] a) M. V. Vasylyev, R. Neumann, *J. Am. Chem. Soc.* **2004**, *126*, 884–890; b) A. Nisar, X. Wang, *Dalton Trans.* **2012**, *41*, 9832–9845.
- [5] a) N. Mizuno, S. Uchida, K. Kamata, R. Ishimoto, S. Nojima, K. Yonehara, Y. Sumida, *Angew. Chem.* **2010**, *122*, 10168–10172; *Angew. Chem. Int. Ed.* **2010**, *49*, 9972–9976; b) S. Uchida, K. Kamata, Y. Ogasawara, M. Fujita, N. Mizuno, *Dalton Trans.* **2012**, *41*, 9979–9983.
- [6] a) Q. Zhang, S. Zhang, Y. Deng, *Green Chem.* **2011**, *13*, 2619–2637; b) J. P. Hallett, T. Welton, *Chem. Rev.* **2011**, *111*, 3508–3576.
- [7] a) Z. Ma, J. Yu, S. Dai, *Adv. Mater.* **2010**, *22*, 261–285; b) E. Ahmed, M. Ruck, *Angew. Chem.* **2012**, *124*, 314–316; *Angew. Chem. Int. Ed.* **2012**, *51*, 308–309; c) H. Fu, C. Qin, Y. Lu, Z.-M. Zhang, Y.-G. Li, Z.-M. Su, W.-L. Li, E.-B. Wang, *Angew. Chem.* **2012**, *124*, 8109–8113; *Angew. Chem. Int. Ed.* **2012**, *51*, 7985–7989; d) Y. Zhao, J. Zhang, B. Han, J. Song, J. Li, Q. Wang, *Angew. Chem.* **2011**, *123*, 662–665; *Angew. Chem. Int. Ed.* **2011**, *50*, 636–639.
- [8] a) A. B. Bourlinois, K. Raman, R. Herrera, Q. Zhang, L. A. Archer, E. P. Giannelis, *J. Am. Chem. Soc.* **2004**, *126*, 15358–15359; b) Y. Zhang, Y. Shen, J. Yuan, D. Han, Z. Wang, Q. Zhang, L. Niu, *Angew. Chem.* **2006**, *118*, 5999–6002; *Angew. Chem. Int. Ed.* **2006**, *45*, 5867–5870; c) P. G. Rickert, M. R. Antonio, M. A. Firestone, K. A. Kubatko, T. Szreder, J. F. Wishart, M. L. Dietz, *J. Phys. Chem. B* **2007**, *111*, 4685–4692.
- [9] a) L. Liu, C. Chen, X. Hu, T. Mohamood, W. Ma, J. Lin, J. Zhao, *New J. Chem.* **2008**, *32*, 283–289; b) S. Wang, W. Liu, Q. Wan, Y. Liu, *Green Chem.* **2009**, *11*, 1589–1594; c) L. Gharnati, O. Walter, U. Arnold, M. Döring, *Eur. J. Inorg. Chem.* **2011**, 2756–2762.
- [10] a) Y. Qiao, Z. Hou, H. Li, Y. Hu, B. Feng, X. Wang, L. Hua, Q. Huang, *Green Chem.* **2009**, *11*, 1955–1960; b) H. Li, Z. Hou, Y. Qiao, B. Feng, Y. Hu, X. Wang, X. Zhao, *Catal. Commun.* **2010**, *11*, 470–475.
- [11] a) Y. Leng, J. Wang, D. Zhu, X. Ren, H. Ge, L. Shen, *Angew. Chem.* **2009**, *121*, 174–177; *Angew. Chem. Int. Ed.* **2009**, *48*, 168–171; b) W. Zhang, Y. Leng, P. Zhao, J. Wang, D. Zhu, J. Huang, *Green Chem.* **2011**, *13*, 832–834; c) Y. Leng, J. Wang, D. Zhu, M. Zhang, P. Zhao, Z. Long, J. Huang, *Green Chem.* **2011**, *13*, 1636–1639; d) P. Zhao, M. Zhang, Y. Wu, J. Wang, *Ind. Eng. Chem. Res.* **2012**, *51*, 6641–6647; e) P. Zhao, Y. Leng, M. Zhang, J. Wang, Y. Wu, J. Huang, *Chem. Commun.* **2012**, *48*, 5721–5723; f) M. Zhang, P. Zhao, Y. Leng, G. Chen, J. Wang, J. Huang, *Chem. Eur. J.* **2012**, *18*, 12773–12782.
- [12] a) N. M. M. Mateus, L. C. Branco, N. M. T. Lourenço, C. A. M. Afonso, *Green Chem.* **2003**, *5*, 347–352; b) Y. Gao, S. W. Arritt, B. Twamley, J. M. Shreeve, *Inorg. Chem.* **2005**, *44*, 1704–1712.
- [13] a) X.-Y. Dou, J.-Q. Wang, Y. Du, E. Wang, L.-N. He, *Synlett* **2007**, 3058–3062; b) Y. Jin, S. Fang, L. Yang, S. Hirano, K. Tachibana, *J. Power Sources* **2011**, *196*, 10658–10666; c) G. V. S. M. Carrera, R. F. M. Frade, J. Aires-de-Sousa, C. A. M. Afonso, L. C. Branco, *Tetrahedron* **2010**, *66*, 8785–8794;

- d) J. Liu, F. Wang, Z. Li, J. Zhou, J. Chen, C. Xia, *Struct. Chem.* **2011**, *22*, 1119–1130.
- [14] a) P. J. Cordeiro, T. D. Tilley, *ACS Catal.* **2011**, *1*, 455–467; b) F. Xiao, B. Xie, H. Zhang, L. Wang, X. Meng, W. Zhang, X. Bao, B. Yilmaz, U. Müller, H. Gies, H. Imai, T. Tatsumi, D. D. Vos, *ChemCatChem* **2011**, *3*, 1442–1446.
- [15] K. Kamata, T. Hirano, S. Kuzuya, N. Mizuno, *J. Am. Chem. Soc.* **2009**, *131*, 6997–7004.
- [16] L. A. Pérez-Maqueda, E. Matijevic, *Chem. Mater.* **1998**, *10*, 1430–1435.
- [17] X. Yan, P. Zhu, J. Fei, J. Li, *Adv. Mater.* **2010**, *22*, 1283–1287.
- [18] T. Okuhara, T. Nakato, *Catal. Surv. Jpn.* **1998**, *2*, 31–44.
- [19] Y. Jiang, S. Liu, S. Li, J. Miao, J. Zhang, L. Wu, *Chem. Commun.* **2011**, *47*, 10287–10289.
- [20] G. Ranga Rao, T. Rajkumar, B. Varghese, *Solid State Sci.* **2009**, *11*, 36–42.
- [21] M. Misono, *Catal. Rev. Sci. Eng.* **1987**, *29*, 269–321.
- [22] I. Holclajtner-Antunović, D. Bajuk-Bogdanović, A. Popa, S. Uskoković-Marković, *Inorg. Chim. Acta* **2012**, *383*, 26–32.
- [23] J. C. Duhacek, D. C. Duncan, *Inorg. Chem.* **2007**, *46*, 7253–7255.
- [24] D. J. Heldebrant, P. K. Koech, M. Trisha C. Ang, C. Liang, J. E. Rainbolt, C. R. Yonker, P. G. Jessop, *Green Chem.* **2010**, *12*, 713–721.
- [25] F. Bellina, C. Chiappe, M. Lessi, *Green Chem.* **2012**, *14*, 148–155.
- [26] T. Yamase, *Chem. Rev.* **1998**, *98*, 307–325.
- [27] M. Guidotti, C. Pirovano, N. Ravasio, B. Lázaro, J. M. Fraile, J. A. Mayoral, B. Coq, A. Galarneau, *Green Chem.* **2009**, *11*, 1421–1427.
- [28] a) O. A. Kholdeeva, N. V. Maksimchuk, G. M. Maksimov, *Catal. Today* **2010**, *157*, 107–113; b) Y. Ding, W. Zhao, H. Hua, B. Ma, *Green Chem.* **2008**, *10*, 910–913; c) L. Hua, Y. Qiao, Y. Yu, W. Zhu, T. Cao, Y. Shi, H. Li, B. Feng, Z. Hou, *New J. Chem.* **2011**, *35*, 1836–1841.
- [29] a) Y. Liu, K. Murata, T. Hanaoka, M. Inaba, K. Sakanishi, *J. Catal.* **2007**, *248*, 277–287; b) L. Nakka, J. E. Molinari, I. E. Wachs, *J. Am. Chem. Soc.* **2009**, *131*, 15544–15554; c) Y. M. A. Yamada, C. K. Jin, Y. Uozumi, *Org. Lett.* **2010**, *12*, 4540–4543.
- [30] T. Mallat, A. Baiker, *Catal. Sci. Technol.* **2011**, *1*, 1572–1583.
- [31] P. G. Jessop, *Green Chem.* **2011**, *13*, 1391–1398.
- [32] W. Fan, P. Wu, T. Tatsumi, *J. Catal.* **2008**, *256*, 62–73.
- [33] a) Y. Ishii, K. Yamawaki, T. Ura, H. Yamada, T. Yoshida, M. Ogawa, *J. Org. Chem.* **1988**, *53*, 3581–3593; b) D. C. Duncan, R. C. Chambers, E. Hecht, C. L. Hill, *J. Am. Chem. Soc.* **1995**, *117*, 681–691; c) R. Prabhakar, K. Morokuma, C. L. Hill, D. G. Musaev, *Inorg. Chem.* **2006**, *45*, 5703–5709; d) K. Kamata, M. Kotani, K. Yamaguchi, S. Hikichi, N. Mizuno, *Chem. Eur. J.* **2007**, *13*, 639–648; e) K. Kamata, R. Ishimoto, T. Hirano, S. Kuzuya, K. Uehara, N. Mizuno, *Inorg. Chem.* **2010**, *49*, 2471–2478.
- [34] N. S. Antonova, J. J. Carbó, U. Kortz, O. A. Kholdeeva, J. M. Poblet, *J. Am. Chem. Soc.* **2010**, *132*, 7488–7497.
- [35] A. Berkessel, J. A. Adrio, *J. Am. Chem. Soc.* **2006**, *128*, 13412–13420.
- [36] M. Ziolek, *Catal. Today* **2004**, *90*, 145–150.
- [37] C. L. Hill, *J. Mol. Catal. A* **2007**, *262*, 2–6.
- [38] D. Demberelnyamba, S. J. Yoon, H. Lee, *Chem. Lett.* **2004**, *33*, 560–561.
- [39] Z. Wang, Y. Cui, Z. Xu, J. Qu, *J. Org. Chem.* **2008**, *73*, 2270–2274.
- [40] L. C. Branco, J. N. Rosa, J. J. Moura Ramos, C. A. M. Afonso, *Chem. Eur. J.* **2002**, *8*, 3671–3677.

Received: January 30, 2013

Published online on April 26, 2013